Journal of Non-Crystalline Solids 610 (2023) 122305

Contents lists available at ScienceDirect

Journal of Non-Crystalline Solids

journal homepage: www.elsevier.com/locate/jnoncrysol

A practical analysis for decelerated growth processes to get physically meaningful kinetic parameters from classical nucleation and growth theory despite of overgrowth

J.S. Blázquez [a,*], R. Caballero-Flores [a], A.F. Manchón-Gordón [b], J.M. Borrego [a], C.F. Conde [a]

[a] Departamento de Física de la Materia Condensada, ICMSE-CSIC, Universidad de Sevilla, P.O. Box 1065, 41080, Sevilla, Spain
[b] Instituto de Ciencia de Materiales de Sevilla, ICMSE CSIC-Universidad de Sevilla, C. Américo Vespucio 49, Sevilla, 41092, Spain

ARTICLE INFO

Keywords:
KJMA or JMAK analysis
Nucleation and growth kinetics
Overgrowth
Avrami exponent
Avrami-Erofeev equation

ABSTRACT

We have analyzed the overgrowth problem arising in decelerated growth processes of spherical crystals in the frame of classical nucleation and growth theory developed by Kolmogorov, Johnson and Mehl, and Avrami (KJMA). To do that, simulations of decelerated growth transformations with a constant nucleation rate have been performed, changing the linear growth rate of spherically shaped nuclei from null (instantaneous growth rate) to constant (characteristic of interface controlled growth processes). We propose the determination of the actual kinetic parameters through the analysis of the inflection point of time evolution of transformed fraction. The correlations found between the effective kinetic parameters from direct KJMA analysis and the actual ones make it possible obtaining physically meaningful parameters. The proposed analysis has been applied to the nanocrystallization of amorphous FINEMET-type compositions.

1. Introduction

The classical theory of nucleation and growth developed by Kolmogorov [1], Johnson and Mehl [2], and Avrami [3] (KJMA) is widely extended to analyze the transformation kinetics of many different solid state transformations [4], even though the premises required for the applicability of KJMA theory are strict (summarized in the five postulates of Kolmogorov [5]).Briefly, KJMA theory stablishes a statistical relationship between the actual transformed fraction, X, and the so-called extended transformed fraction, X_{ext}, which corresponds to the transformed fraction in the absence of any impingement between the different growing nuclei. Using statistical arguments, KJMA theory assumes that the relationship between both magnitudes is:

$$\frac{dX}{dX_{ext}} = 1 - X. \tag{1}$$

In the early stages of transformation $X \ll 1$ and, therefore, $X \sim X_{ext}$, whereas at the final stages of transformation, despite X_{ext} keeps growing beyond 1, X saturates.

The great advantage of this description is that X_{ext} can be easily calculated assuming the laws governing the nucleation and growth rates. In general, it can be considered a constant nucleation rate I and a power law for the linear growth rate such as $\frac{dR(t,\tau)}{dt} = G(t-\tau)^{g-1}$. In the previous expression, $R(t,\tau)$ is the radius at time t of a spherical crystal nucleated at time $\tau < t$, g the growing exponent, and G a constant of the kinetic process. When $g = 1$, G becomes the constant linear growth rate of an interface controlled growth process. When $g = 1/2$, the growth law is characteristic of a diffusion controlled decelerated growth process, being $G = \sqrt{2D}$, with D the corresponding diffusion coefficient. Finally, when $g = 0$, and thus, $G = 0$, the growth rate is null and an instantaneous growth process is described (the growth is so sudden to the final size that crystals appear with their final size and further growth is absent). Taking this into account, X_{ext} can be calculated as:

$$X_{ext} = [k(t - t_0)]^n, \tag{2}$$

where $n = 3g + 1$ is the Avrami exponent particularized for three dimensional growth and constant nucleation rate and t_0 is the induction time. The frequency factor is $k = \sqrt[n]{4\pi I (G/g)^3/3(g+1)}$ for $g > 0$ or $k = \sqrt[n]{4\pi I R_{nuc}^3/3}$ for $g = 0$ [4], with R_{nuc} the radius of the nuclei (which was neglected for $g > 0$). Eq. (2) can be substituted in Eq. (1) and, after integration, leads to the well-known KJMA equation:

* Corresponding author
E-mail address: jsebas@us.es (J.S. Blázquez).

https://doi.org/10.1016/j.jnoncrysol.2023.122305
Received 15 February 2023; Received in revised form 16 March 2023; Accepted 17 March 2023
Available online 28 March 2023

$$X = 1 - exp\{-[k(t-t_0)]^n\}. \quad (3)$$

This equation predicts linearity between $ln(-ln(1-X))$ and $ln(t-t_0)$ and, consequently, the values of n and k can be easily obtained from its slope and its intercept. This simple analysis makes the Avrami plot a very attractive way to easily acquire kinetic parameters, leading to its extensive use found in the literature (e. g. a search of "Avrami exponent" [1] in Web of Science platform leads to more than 2500 entries and more than 2800 in Scopus). However, KJMA theory is not always directly applicable to nucleation and growth based transformations. Particularly, the variation of kinetic parameters along the transformation, as it occurs for non-isothermal regimes, has not been taken into account in KJMA theory [4]. On the other hand, it has been also shown that KJMA theory cannot be directly applied to analyze nanocrystallization processes [6], transformation that involves simultaneous processes [7], the mechanical amorphization [8] or martensitic transformations [9]. In the case of decelerated growth processes, they deviate from KJMA predictions due to the overgrowth produced by phantom nuclei, which, in the frame of extended transformation, are those nuclei statistically appearing in an already transformed region and thus contributing to X_{ext} but not to X.

The KJMA theory accounts for the formation of phantom nuclei only when the phantom crystal is always within the transformed region [10]. However, this is not the case when the linear growth rate decelerates with time, as it occurs in diffusion controlled processes. In decelerated growth processes, a phantom nucleus formed close enough to the boundary of the already transformed region can grow beyond that boundary, leading to an overgrowth region that KJMA theory is not able to account for (i.e. statistically it would erroneously contribute to X).

Different authors have afforded the overgrowth problem in order to propose a better description of decelerated processes [11]. In particular, Tomellini and Fanfoni [12] have mathematically solved the problem using a correlation function between nuclei to avoid the formation of phantom ones. However, these analyses do not yield the research community to abandon Avrami plot in benefit of a more correct analysis. This is because of the easy and straightforward character of the analysis by direct application of KJMA theory, which allows for a fast classification of the transformation of interest with respect to its Avrami exponent. Once KJMA theory is not valid for a certain transformation, Avrami exponent is just an effective value and loses its physical meaningful relationship with nucleation and growth mechanisms.

In this work, we have analyzed the overgrowth problem characteristics of the decelerated growth processes in the frame of the KJMA theory. Particularly, we have phenomenologically explored the effect of overgrowth on the deviation of actual kinetics from KJMA theory through different simulations of nucleation and growth processes of spherical crystallites with growth exponent $g \leq 1$. The predictions of the proposed analysis have been compared to experimental results derived from isothermal nanocrystallization of amorphous FINEMET alloys. The correlations found between the actual kinetic parameters and the effective ones supply a practical tool to recover the physical meaning of the corresponding kinetic parameters.

2. Simulations

Simulations were performed by building up a MatLab script (MatLab R2022b, MathWorks) consisting on a cubic space of size L defined with periodic boundaries. Time is discretized in iteration steps. In every iteration step, a new nucleus with an initial radius R_0 is created in a random position ($I = L^{-3}$ per iteration step). This nucleation position is checked whether it is in an already transformed region or not, and correspondingly labelled as phantom nucleus or real one. Moreover, all the already formed nuclei (independently whether they are phantom or not) are allowed to grow further following a power law $R(t,\tau) = R_{nuc} + R_0\left(\frac{t-\tau}{\Delta t}\right)^g$, only valid for $t > \tau$; $t/\Delta t$ is the iteration step and $\tau/\Delta t$ is the iteration step at which the corresponding crystal was nucleated. Therefore, time dimension is explicitly used assigning a time Δt for an iteration step. The radius of the nucleus $R_{nuc} \sim 0$ is neglected when $g > 0$ and thus when $g = 0$, $R(t,\tau) = R_{nuc}$ is constant. This leads to an extended fraction, which can be analytically calculated as:

$$X_{ext} = \frac{4\pi R_0^3}{3L^3}\left(\frac{t}{\Delta t}\right)^{3g+1}. \quad (4)$$

In every iteration step we proceed to check both actual transformed fraction and the overgrowth one. In order to do so, we check for 100 random points in the explored volume whether each point is either in an already transformed region covered by at least a real crystal (contributing to X), or it is in a region only covered due to the growth of a phantom nuclei (contributing to overgrowth, X_{over}), or it is in an untransformed region. Normalizing the number of points contributing to each one to the number of checked points leads to the corresponding values of $X(t)$ and $X_{over}(t)$. In order to obtain statistically significant values of $X(t)$ and $X_{over}(t)$, the simulation was repeated and the average over 100-500 curves was taken as the signal to be analyzed. In a single simulation we can reduce the noise to signal ratio by increasing the number of checked points to estimate the transformed fractions (real and overgrowth ones). However, it is worth mentioning that a single simulation is not statistically significant (i.e. it should be possible, for a particular simulation event, that nuclei appear very close between them and leading to fortuitously high overgrowth fraction). Therefore, instead of increasing the number of checking points over 100, we found a better solution to increase the number of simulated curves (up to 500 was taken) to obtain the average values.

Fig. 1(a) shows the plot of $X_{over}(t)$ as a function of $X(t)$ for $0 \leq g \leq 1$. As can be seen, overgrowth is null for $g = 1$ and almost negligible for $g \geq 0.5$ (< 1 %) but it reaches 13 % in the case of $g = 0$. Figs. 1(b,c) show, as examples, $X(t)$ and the theoretical prediction from KJMA, $X_{KJMA}(t)$, along with the addition $X_{plus}(t) = X_{over}(t) + X(t)$. It could be observed that $X_{KJMA} = X_{plus}$ independently of the simulation parameters. The only difference is that X_{KJMA} is analytically calculated (see Eq. 3) and thus smooth, whereas X_{plus}, as an experimental result from simulations, is noisy.

Figs. 2(a,b) show the Avrami plot applied to $X(t)$ for $g = 0$ and $g = 0.5$ (corresponding $X(t)$ curves are shown in Figs. 1(b,c)). Independently of g, Avrami plot applied to X_{plus} exactly follows KJMA theory, and both the slope and the intercept agree with the Avrami exponent, $n_{plus} = 1 + 3g$, and the frequency factor, $lnk_{plus} = ln\left(\frac{4\pi R_0^3}{3L^3}\right)$ (as expected from Fig. 1). In Fig. 2 we discuss that this does not occur when we study the Avrami plot applied to $X(t)$ due to overgrowth of KJMA theory. In fact, when Avrami plot is applied to $X(t)$, deviations from linearity appear for $g \geq 0.5$ (i.e. $n \geq 2.5$), although they are not significant, in agreement with the reported validity of KJMA theory to describe diffusion controlled growth processes despite the overgrowth problem [13,14]. However, in strongly impinged growth processes, there is a clear deviation from linearity and a double slope behavior is appreciated, as can be observed in Fig. 2(a), which is widely described in the literature for experimental data of nanocrystallization [15–17]. In order to quantify this mentioned double slope behavior in the Avrami plot, we have obtained three values of the Avrami exponent: the maximum value, n_1, associated with the first branch of the curve, i.e., when we use the range $0.1 < X(t) < 0.5$ to perform the fitting; the minimum value, n_2, associated with the second branch of the curve, i.e., when we use the range $0.5 < X(t) < 0.9$ to perform the fitting; and finally, the medium value, n_m, associated with the whole curve, i.e., when we use the range $0.1 < X(t) < 0.9$ to perform the fitting (values below 0.1 and above 0.9 are excluded taking into account that they can be strongly affected by baseline in experimental data). The comparison between the overgrowth corrected n_{plus} and the

[1] Date of search: November 28th 2022.

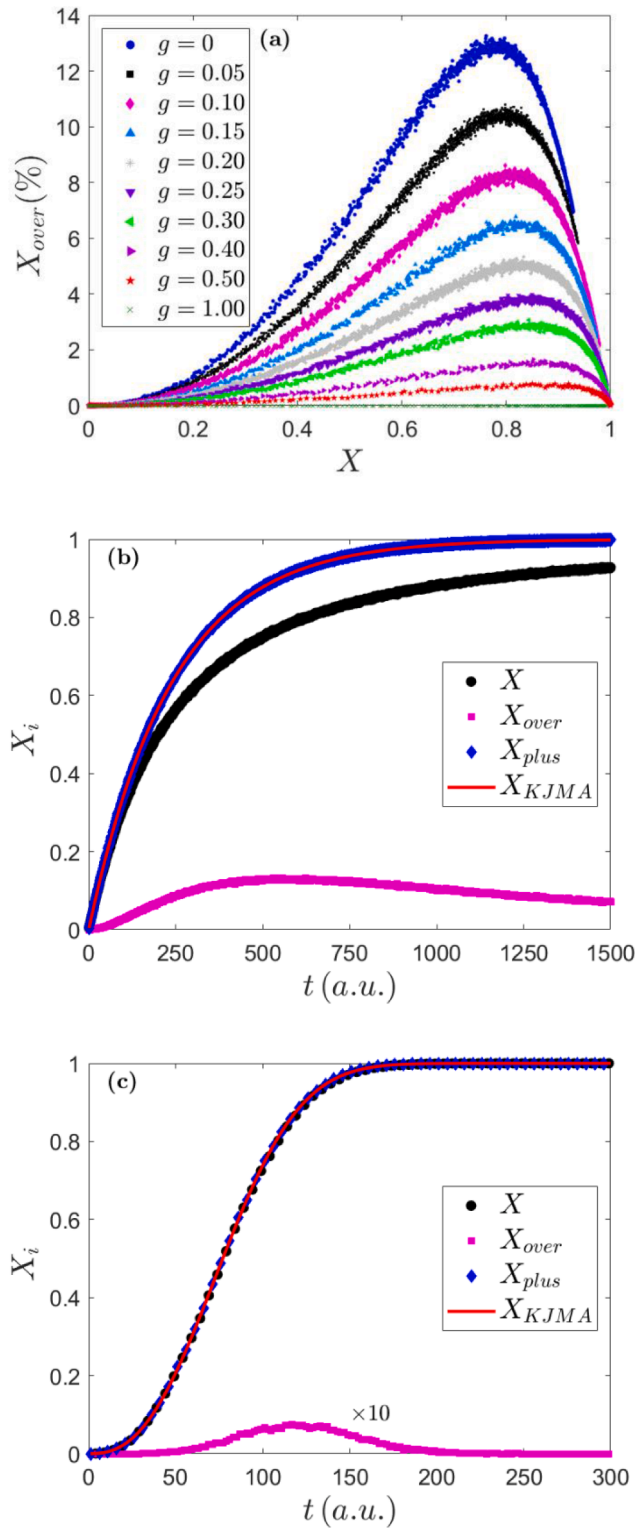

Fig. 1. $X_{over}(t)$ as a function of $X(t)$ for $0 \le g \le 1$ (a). Actual transformed fraction, $X(t)$, overgrowth, $X_{over}(t)$, addition $X_{plus}(t) = X_{over}(t) + X(t)$, and theoretical prediction from KJMA theory, $X_{KJMA}(t)$, for $g = 0$ (b) and $g = 0.5$ (c). In panel (c) the overgrowth fraction has been increased 10 times for the sake of clarity.

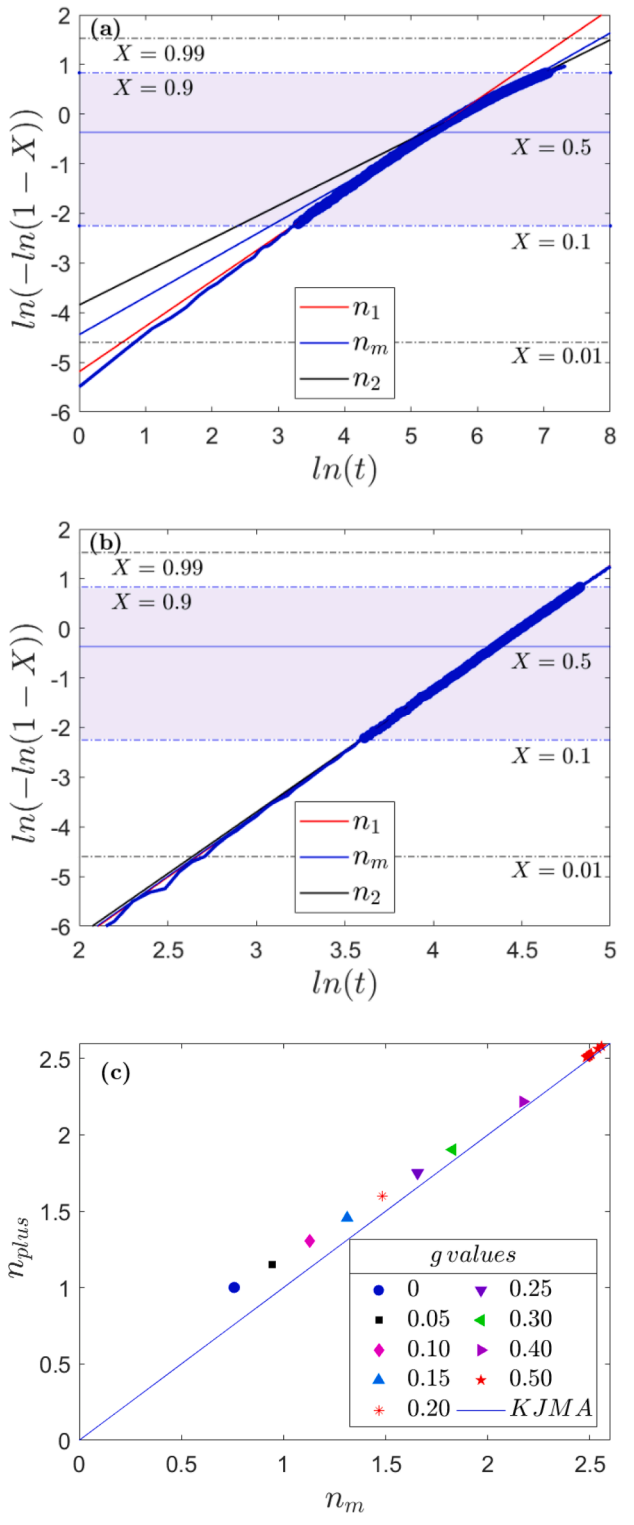

Fig. 2. Avrami plot for two different values of the growing exponent, $g = 0$ (a) and $g = 0.5$ (b). The horizontal lines indicate values of X(t) = 0.01, 0.1, 0.5, 0.9 and 0.99, and the shaded areas the whole range of $0.1 < X(t) < 0.9$ where we have performed the three fittings of n_1, n_2 and n_m. Comparison between the Avrami exponents given by the KJMA theory, n_{plus}, and the one obtained when the overgrowth is considered, n_m (c).

non-corrected n_m, is presented in Fig. 2(c), showing that Avrami exponent should be underestimated as $n_m < n_{plus}$ but these values asymptotically tend to be equal as g approaches 1 and become almost equal at $g = 0.5$.

To account for a stronger impingement than that considered by KJMA theory, some authors proposed a modification of Eq. (1) [18]:

$$\frac{dX}{dX_{ext}} = (1-X)^{\gamma}, \tag{5}$$

with γ the impingement parameter. In the following, the actual transformed fraction following Eq. (5) will be denoted as X_γ and that obtained from Eq. (1) is X_{plus}. The analytical expression for X_γ as a function of X_{ext} is [18]:

$$X_{ext} = \frac{1-\left(1-X_\gamma\right)^{1-\gamma}}{1-\gamma} \rightarrow X_\gamma = 1-[1-(1-\gamma)X_{ext}]^{\frac{1}{1-\gamma}}. \tag{6}$$

Using Eqs. 5 and 6 we can obtain an analytical expression for the theoretical overgrowth depending on γ as $X^{\gamma}_{over} = X_{plus} - X_\gamma$ (analogously to $X_{over} = X_{plus} - X$). Fig. 3 shows a direct comparison between X^{γ}_{over} and X_{over} values as a function of the corresponding transformed fraction X. The data displayed correspond to the best fitted γ values of simulated X_{over} curves using different values of g indicated in Fig. 1(a).

It is worth mentioning that departure from KJMA theory due to overgrowth in decelerated processes could be approximately described by Eq. (5) only for $\gamma \leq 1.57$. Therefore, kinetic processes described by higher values of γ do not respond to classical KJMA premises including overgrowth correction in decelerated growth processes. This is, for example, the case of Austin-Rickett classical kinetic equation that is equivalent to Eq. (5) with $\gamma = 2$ [19], or Tagami and Tanaka equation with $\gamma = 1+\eta$ when $\eta > 0.57$ [20]. Fig. 4 shows the correlation of γ parameter and the theoretical $n_{plus} = 1+3g$ value after fitting simulated X curves to X_γ for the range $0.1 < X < 0.9$. Therefore, one possible analysis to acquire the physical meaningful Avrami exponent could be, firstly, to fit experimental X data to X_γ and, secondly, from the obtained γ value and the correlation shown in Fig. 4, actual $n = n_{plus}$ could be inferred. However, this analysis should require a well-defined transformation curve, which is not always available, and thus a simple and more robust analysis is proposed following the direct application of Avrami plot to the experimental data. From the linear fitting of the Avrami plot, we obtain an effective Avrami exponent, n_{eff}, and an effective frequency parameter, k_{eff}, that can be compared in our simulations to the actual values of n_{plus} and $k_r = k_{eff}/k_{plus}$, respectively. Moreover, these values can be recovered for our simulations from the linear fitting of Avrami plot applied to X_{plus}, which shows that the deviation due to noise is negligible.

Therefore, Fig. 5 shows the relationships between n_{eff} and the ratio of k_{eff}/k_{plus} (from Avrami plot applied to the range $0.1 < X(t) < 0.9$) with the actual value of $g \leq 0.5$, with $n_{plus} = 1+3g$. The following linear equations are fitted to the simulation results:

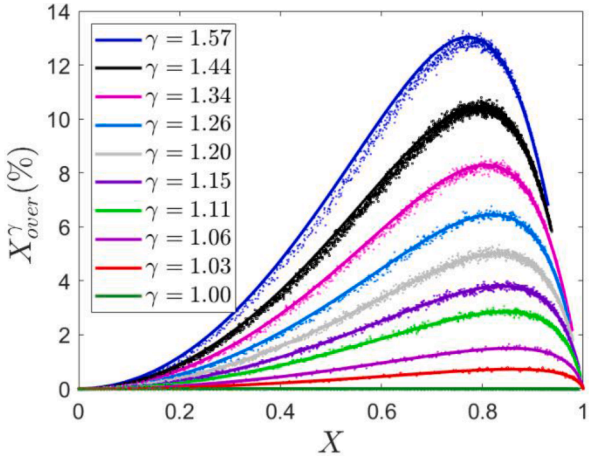

Fig. 3. Comparison of $X^{\gamma}_{\rm over}$ vs. X as a function of γ (solid lines) with $X_{\rm over}$ vs. X as a function of g (symbols). The color code used in this figure is the same than the one used in Fig. 1(a).

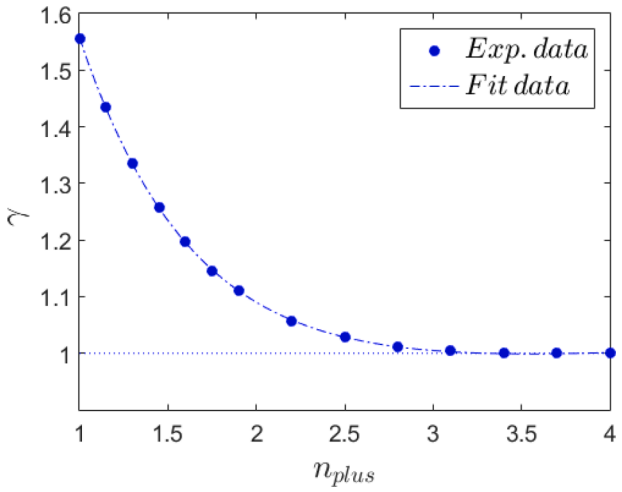

Fig. 4. Correlation between γ and $n_{\rm plus} = 1+3g$. The fitting has been obtained with the sum of two exponential functions, i.e., $\gamma = a\exp(-bn_{\rm plus}) + c\exp(dn_{\rm plus})$ with a = 2.89(8), b = 1.55(4), c = 0.92(2), and d = 0.019(4).

$$(0.1 < X < 0.5) \rightarrow n_1 = 3.197(16)g + 0.915(4), \tag{7a}$$

$$(0.1 < X < 0.9) \rightarrow n_m = 3.49(6)g + 0.777(15), \tag{7b}$$

$$(0.5 < X < 0.9) \rightarrow n_2 = 3.64(4)g + 0.670(9). \tag{7c}$$

Whereas there is a trend $1+3g = n_{plus} \geq n_1 \geq n_m \geq n_2$, this is not the case found for the normalized frequency factors, and k_{rm} is not in between k_{r1} and k_{r2} but, although all values are below 1, k_{rm} is the lowest and k_{r1} is the highest, independently of g. It must be taken into account that Eq. (2) was defined to preserve the $time^{-1}$ dimensionality of the frequency factor and it yields that the intercept in Avrami plot corresponds to $y_{0i} = n_i \ln k_i$. Thus, although $y_{0plus} \leq y_{01} \leq y_{0m} \leq y_{02}$, the dependence of $k_{ri} = (1/k_{plus})e^{y_{0i}/n_i}$ on n_i affects the trend. As it is generally accepted, the highest uncertainty on kinetic experiments corresponds to the determination of the induction time or the final transformed fraction. Thus, in order to circumvent these limitations on the analysis of the data a specific range (abovementioned used to determine n_1, n_m and n_2) should be selected. The obtained results constitute a very simple method for the determination of the physical meaningful parameters of KJMA theory in decelerated growth processes.

A further result can be predicted from the performed simulations: the evolution of the crystal size with time during isothermal treatment and its relation with the growth exponent. From the simulation results, we can obtain the average radius of the crystallites as:

$$\langle R\rangle \sim \sqrt[3]{\langle R^3\rangle} = L\left(\frac{3}{4\pi}\frac{X}{N_{nuc}}\right)^{1/3}, \tag{8}$$

where N_{nuc} is the number of real nuclei formed. The time evolution of the average radius, $\langle R\rangle \sim \sqrt[3]{\langle R^3\rangle}$, cannot be compared with a theoretical law $\langle R(t)\rangle \sim R_{eff}(t-t_0)^{g_{eff}}$, except for very low times. In any case, $g_{eff} < g$ as the average size is referred to the induction time and new but smaller crystals are continuously nucleating. Moreover, when the geometrical impingement becomes significant, crystal size saturates, as it can be observed in Fig. 6. The average crystal volume, $\langle V_{cr}\rangle = \frac{4}{3}\pi\langle R^3\rangle$, is also shown.

Even though, some information could be obtained from the evolution of $\langle R\rangle$ with time after developing the dependence of N_{nuc} assuming a constant nucleation rate I. In this case:

$$N_{nuc}(t) = \int_{t_0}^{t} I(1-X)L^3 dt, \tag{9}$$

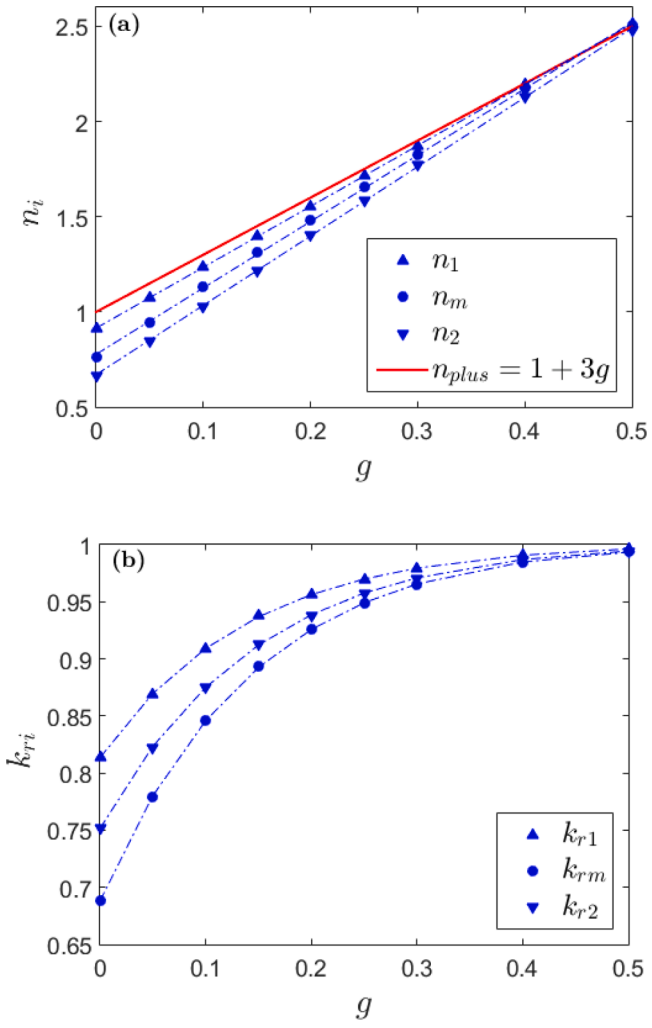

Fig. 5. The values of the Avrami exponents $n_1 \geq n_m \geq n_2$ along with $n_{\text{plus}} = 1 + 3g$ (red line (a), and reduced frequencies k_{r1}, k_{rm}, k_{r2} (b) obtained from the three defined X ranges as a function of the growing exponent g. Linear fitting has been used to fit symbols in (a) (See Eqs. 7(a − c)), and the sum of two exponential functions in (b), i.e.$k_{\text{ri}} = a_i\exp(-b_i g) + c_i\exp(d_i g)$ with $a_1 = -0.190(14)$, $b_1 = 7.0(6)$, $c_1 = 1.003(15)$, and $d_1 = 0.002(3)$; $a_m = -0.33(2)$, $b_m = 6.6(4)$, $c_m = 1.019(18)$, and $d_m = -0.03(3)$; $a_2 = -0.261(16)$, $b_2 = 6.5(4)$, $c_2 = 1.013(16)$, and $d_2 = 0.02(3)$ (dashed blue lines).

where it has been taken into account that the available volume for nucleation, $(1 - X)L^3$, is reduced as transformation progresses.

Using the differential form of $\frac{dN_{nuc}(t)}{dt}$ and combining Eqs. 8 and 9 with the average volume of crystals $\langle V_{cr}\rangle = \frac{4}{3}\pi\langle R^3\rangle$, we obtain an expression for the nucleation rate:

$$I = \frac{1}{\langle V_{cr}\rangle(1-X)}\left(\frac{dX}{dt} - \frac{X}{\langle V_{cr}\rangle}\frac{d\langle V_{cr}\rangle}{dt}\right), \tag{10}$$

This expression is independent on g and on whether or not the KJMA theory is followed. Therefore, from the slope of $\frac{dX}{dt} - \frac{X}{\langle V_{cr}\rangle}\frac{d\langle V_{cr}\rangle}{dt}$ vs. $\langle V_{cr}\rangle(1-X)$ it is possible to obtain the value of I. Fig. 7 shows the result of this plot for $g = 0.5$ and different values of R_0 in a explored cubic region of size $L = 10$. As nucleation is allowed to occur at each iteration step, the value of the nucleation rate is $I = L^{-3} = 10^{-3}$ per unit volume and time as the red line in Fig. 7 shows.

Finally, we study the effect of a non-constant nucleation rate on the effective parameters obtained from KJMA analysis. In order to do so, the nucleation in every step is allowed only when a random number between $0 < rand < 1$ fulfills: $rand < (1 - fX)$ where f is a weight factor on

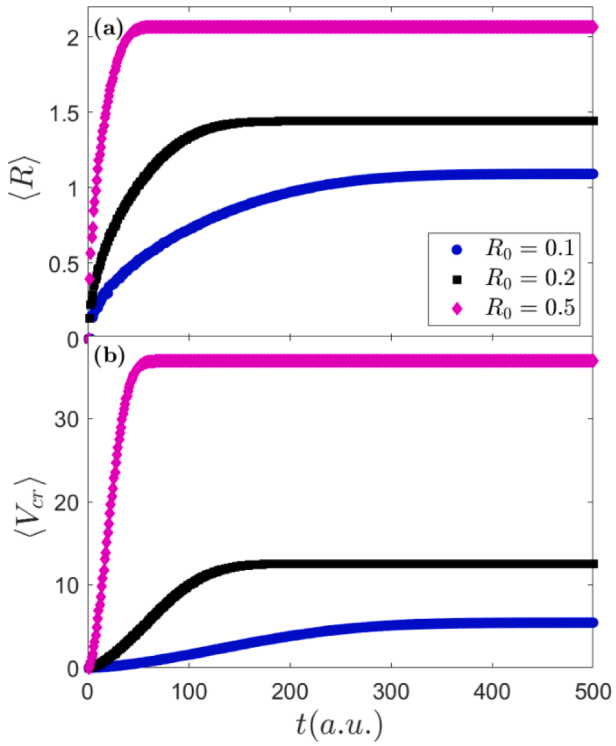

Fig. 6. Time dependence of average crystal radius, $\langle R\rangle$, (a) and average crystal volume, $\langle V_{\text{cr}}\rangle = \frac{4}{3}\pi\langle R^3\rangle$, (b) for simulations performed averaging over 500 curves with $L = 10$, $g = 0.5$ and several values of $R_0 = 0.1,\ 0.2,\ 0.5$. Units are arbitrary in a explored space L^3 with $L = 10$.

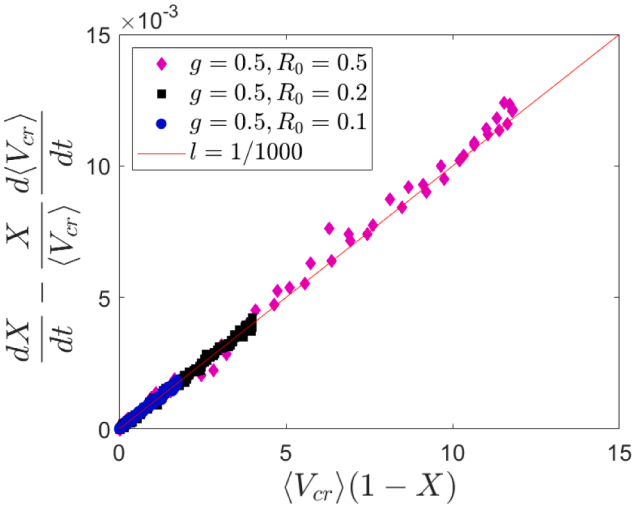

Fig. 7. Representation of linearity predicted from Eq. (10) for $g = 0.5$ and $R_0 = 0.1$, 0.2 and 0.5 The latter parameter is in arbitrary units in an explored space L^3 with $L = 10$. The red line corresponds to the expected linear trend with slope $I = L^{-3} = 10^{-3}$ nuclei per unit volume and time.

the effect the transformed fraction has on the decrease of I (i.e. $f = 1$ for nucleation site saturation at $X = 1$). Fig. 8 shows results from simulations averaging 500 curves ($L = 10$, $g = 0.5$, $R_0 = 0.1$) for the evolution of the transformed fraction, X, (a) and average crystal size, $\langle V_{cr}\rangle$, (b) as a function of time, overgrowth fraction X_{over} vs. X (c), and Avrami plot for three different values of $f = 0,\ 0.5,\ 1$ and 2 (d).

According to Fig. 8, we can observe that the decrease in nucleation rate is not seriously affecting the previous results. Overgrowth slightly decreases as it does effective Avrami exponents from $n_m = 2.47$ for

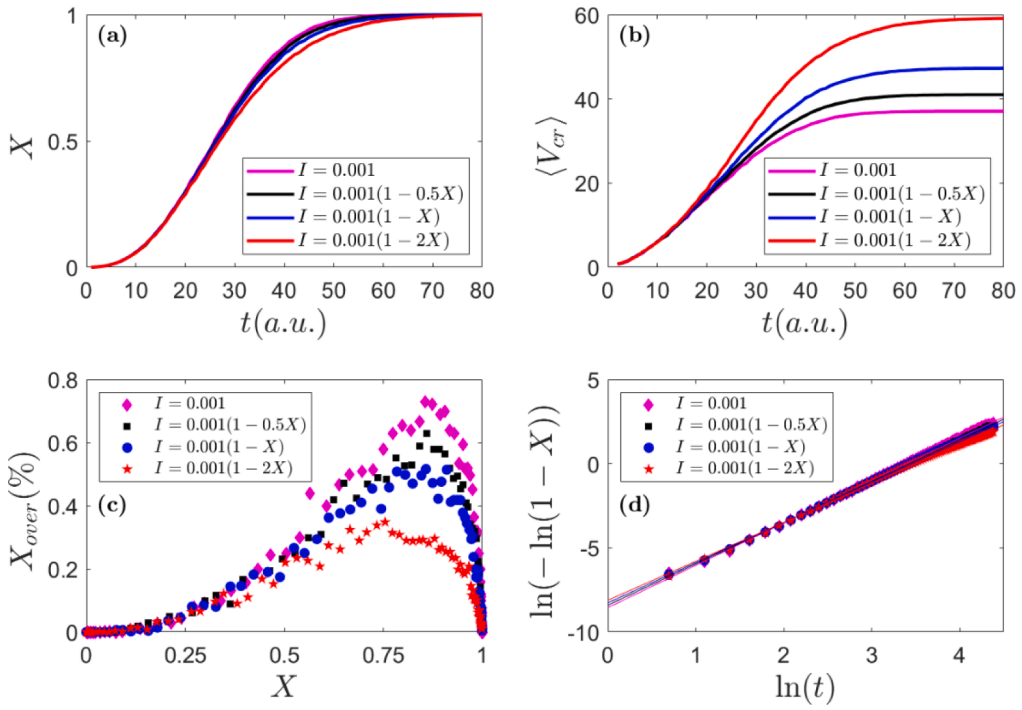

Fig. 8. Transformed fraction, X, (a) and average crystal volume, $\langle V_{cr} \rangle$, (b) as a function of time, overgrowth fraction, X_{over}, as a function of transformed fraction, X, (c) and Avrami plot for simulations performed for $L = 10$, $g = 0.5$, $R_0 = 0.1$ and under different nucleation scenarios: $I = I_0(1 - fX)$, with $f = 0,\ 0.5,\ 1$ and 2 (d). In panel (d), the lines correspond to the linear fitting of each curve corresponding to a f value.

constant nucleation rate $I = I_0$, to $n_m = 2.34$ for $I = I_0(1 - X)$ thus about 5 % (An even lower value of $n_m = 2.21$ is obtained for $I = I_0(1 - 2X)$, for which exhaustion of nucleation sites occurs before the end of the process). The frequency factors differ in an even smaller amount (<1 %). Overgrowth reduces as nucleation rate (source for new phantom nuclei) also reduces. As Avrami exponent (i.e. growth exponent) decreases, the effect maintains the dependence on the transformed fraction. As a limit situation, in the case of instantaneous growth, $g = 0$, it does not matter whether the nucleation rate changes or not, although the process must be delayed in time, the dependence on transformed fraction will be the same.

3. Comparison with experimental data

In order to test the results derived from our simulations, the isothermal nanocrystallization kinetics of two melt-spun amorphous FINEMET type alloys with composition $Fe_{73.5}Si_{16.5-y}B_9Cu_1Nb_y$ ($y = 3$ and 5) has been analyzed. To do that, both amorphous samples were annealed 5 h in a DSC7 Perkin-Elmer calorimeter. In this device, two independent furnaces heating the sample and the reference, respectively, allows for a direct measurement of the heat flow. Annealing was performed at 10 K below the corresponding crystallization onset temperature measured at 20 K/min, in order to study the crystallization process from the initial value of the transformed fraction $X = 0$. As can be determined in Fig. 9(a), these temperatures are 793 K and 828 K for the alloys with 3 and 5 at.% of Nb, respectively. Details on production and microstructure can be found elsewhere for the alloy with 3 at. % of Nb [21]. In that previous work, some of the authors proposed an understanding of the nanocrystallization process as the addition of multiple classical microprocesses. In that case, the limitation of volume available for each individual process led to an effective impingement of the growth that can resemble qualitatively the low Avrami exponents experimentally found. Unfortunately, that interpretation prevents the acquisition of further information from kinetic analysis. However, in this new study we did not impose any volume limitation to any part of the system but the low values of the effective Avrami exponents can be obtained assuming an intrinsic low growth exponent. Moreover, these low growth exponents yield the overgrowth effect that is discussed here. Finally, in the present work we have found correlations between the effective and the actual kinetic parameters that allow us to recover the latter parameters, which are those with physical meaning.

Nucleation in FINEMET alloys is heterogeneous, as formation of Fe(Si) (disordered α or ordered DO_3 phase) is triggered by Cu-clusters, which are randomly distributed in the volume of the sample [22,23]. Therefore, the requirement for random nucleation in KJMA theory is fulfilled by this transformation. Nb and B are insoluble in the nanocrystals and thus must be rejected to the amorphous matrix. However, due to the low diffusivity of Nb, this element piles up at the edge of the nanocrystals constraining their size and enhancing the activation energy for transformation. This low diffusivity leads to a stabilization of the amorphous phase evidenced by the shift of the onset temperature observed in Fig. 9(a) as Nb content increases in the alloy.

Fig. 9 shows the differential scanning calorimetry (DSC) isothermal signals for the as-cast samples (Fig. 9(b)), along with the non-isothermal scans at 20 K/min for the as-cast samples and the samples after the isothermal treatment (Fig. 9(a)). The latter scans evidence a remaining enthalpy of the primary crystallization peak of both as-cast samples ($\Delta H \sim 10$ J/g), which isothermal treatment was not able to complete. This allows us to estimate the enthalpy that must be released during isothermal treatment $\sim 55 - 60$ J/g. Moreover, these data are needed in order to correct the baseline of the isothermal signal in the following way: taking a straight line from a completion time, t_{end}, with the slope of the DSC signal at that time and comparing the area below with the expected one. This shows that $t_{end} \sim 1500$ s. Baseline is one of the major experimental problems to solve when the process is widely extended in time and the procedure followed here is just the simplest approach to assume (a linear drift). Once the baseline is subtracted, transformed fraction can be taken as the normalized integral of the DSC signal, considering two different possibilities: normalizing the enthalpy released to that at t_{end}, thus $X(t_{end}) = 1$ is imposed; or defining $X = \Delta H_{iso}(t)/\Delta H^{Total}_{No-iso}$, where $\Delta H_{iso}(t)$ is the enthalpy released at isothermal

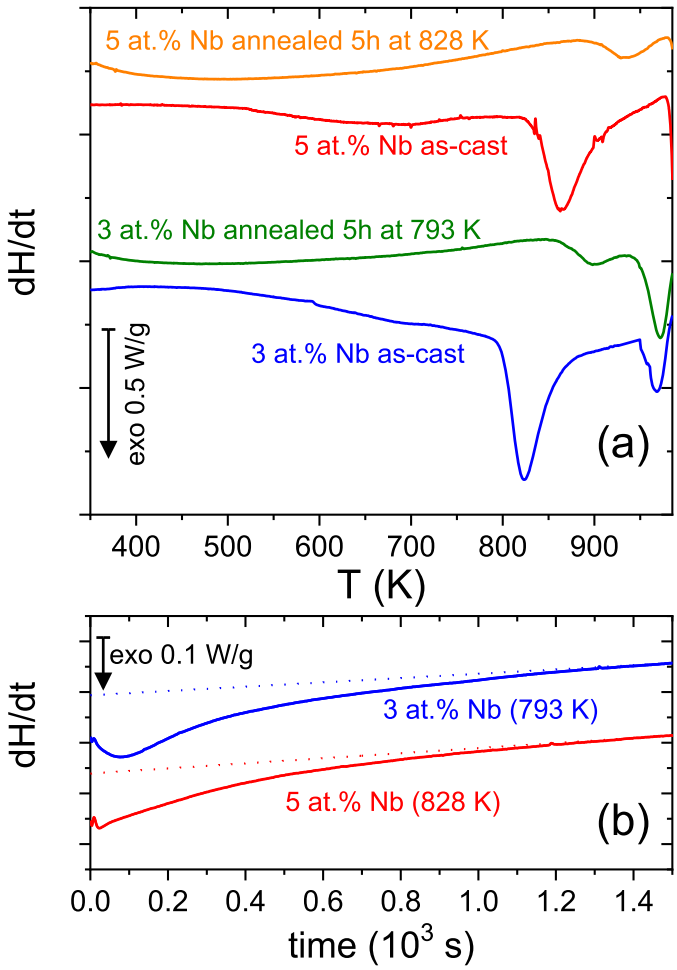

Fig. 9. (a) Non isothermal DSC scans at 20 K/min for as-cast $Fe_{73.5}Si_{16.5-y}B_9Cu_1Nb_y$ (y = 3 and 5) alloys along with those for samples after 5 h isothermal treatment at 10 K below the onset temperature. (b) Isothermal DSC scans of as-cast samples at 10 K below the corresponding onset temperature.

time t and $\Delta H^{Total}_{No-iso}$ is the addition of the enthalpy released at t_{end} plus the remaining enthalpy measured in the following non-isothermal scan, thus $X(t_{end}) < 1$. Taking this into account we delimit the uncertainty in saturation value. The use of this normalization implies the assumption that enthalpy of transformation is directly proportional to the transformed fraction, which must be taken as an approximation as discussed by Fokin et al. [22] and Barandiarán et al. [23].

Once X is experimentally obtained, we proceed to estimate the induction time, t_0, which also has a significant effect in the effective parameters obtained [4]. In order to do so, we take into account that, for KJMA theory, t_0 is related with the inflection point t_{inf} and the induction time estimated from the interception of the steepest line to $X = 0$, t_{slope}, through the Avrami exponent as:

$$t_0 = t_{slope} + 0.57(n-1)\left(t_{inf} - t_{slope}\right). \tag{11}$$

Where the prefactor of the parenthesis has been rounded (with respect to the reported value in the Eq. 18 and Fig. 4 in ref. [4]) to fulfill that $t_0 = t_{slope}$ for $n = 1$. It is worth noting that overgrowth is negligible at the values corresponding to the studied samples, $t_{inf} = 80$ s and $X(t_{inf}) = 0.13$ for the alloy with 3 at.% of Nb, and $t_{inf} = 25$ s and $X(t_{inf}) = 0.04$ for the alloy with 5 at.% of Nb (or 0.15 and 0.05, respectively, when imposing $X(t_{end}) = 1$). This allows us to neglect overgrowth (see Fig. 1) and use KJMA equation for these low values of transformed fractions, thus an Avrami exponent can be inferred from $X(t_{inf})$ as:

$$n = \frac{1}{1 + ln\left(1 - X\left(t_{inf}\right)\right)}. \tag{12}$$

Errors in n obtained in this way can be estimated as $\Delta n = n^2 \Delta X(t_{inf})/(1 - X(t_{inf}))$ which, for low enough values of n, remains low. Finally, values obtained for the two studied alloys are between $n = 1.16$ and 1.19, $(0.053 < g < 0.063)$ for the alloy with 3 at.% of Nb, and $n = 1.04$ and 1.05 $(0.013 < g < 0.016)$, for the alloy with 5 at.% of Nb, depending on the chosen normalization. Error can be estimated ± 0.03 considering a confident $\Delta X(t_{inf}) = 0.02$.

Fig. 10 shows the Avrami plot for both alloys and the two different normalization criteria to obtain X. In the case of normalizing using $X(t_{end}) = 1$, the increase in the slope at long times is indicative of an underestimation of the saturation value. However, when normalizing is done considering the total enthalpy registered in non-isothermal scans, the two slope behavior due to overgrowth predicted by the above simulations are coherent with the estimated Avrami exponents from the analysis of the inflection time. In this case, the process is not fully completed (evidenced by the remaining enthalpy detected in non-isothermal scans) and transformed fraction reaches ~ 0.85 for both alloys during isothermal treatment. Uncertainty in the saturation value makes a more reliable analysis when Avrami plot is fitted in the range $0.1 < X(t) < 0.5$. Table 1 shows the parameters obtained in the corresponding linear fitting.

Using Eq. 7(a), $0.052 < g < 0.071$ and $0.016 < g < 0.029$ values are deduced for the alloys with 3 and 5 at.% of Nb, respectively, in good agreement with the data obtained from the inflexion point. As expected, a lower growth rate is related to the higher content in Nb and the impingement due to the slow diffusion of this element in the matrix piling up at the edge of the growing crystals [24,25]. The obtained ranges for k_1 are $2.2{\cdot}10^{-3} < k_1 < 2.7{\cdot}10^{-3}$ s^{-1}, for 3 at. % Nb alloy, and slightly smaller, $1.6{\cdot}10^{-3} < k_1 < 2.0{\cdot}10^{-3}$ s^{-1}, for 5 at. % Nb alloy. Taking into account the dependence of k_r on g shown in Fig. 5(b), these values would be about 82 % of the actual values of the frequency factors.

In order to check the predictions for the evolution of the average volume of crystallites, we used the experimental data of the crystalline fraction, α_{cr}, and the average crystals size, $\langle V_{cr} \rangle$, results for a FINEMET alloy isothermally treated at 748 K (50 K below the onset temperature of crystallization at 10 K/min) obtained from synchrotron radiation and reported in [26].

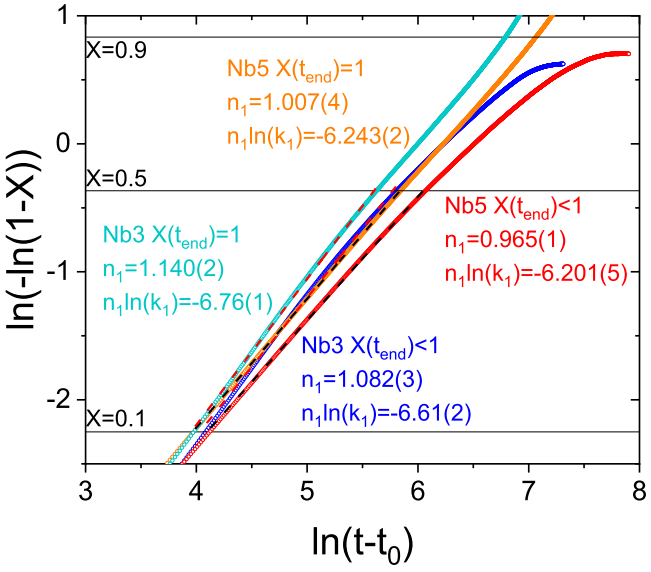

Fig. 10. Avrami plot applied to the isothermal DSC scans of $Fe_{73.5}Si_{16.5-y}B_9Cu_1Nb_y$ ($y = 3$ and 5) alloys shown in Fig. 9(b). Dashed lines are the corresponding linear fittings in the range $0.1 < X(t) < 0.5$.

Table 1
Kinetic parameters obtained from linear fitting of experimental Avrami plot in the range $0.1 < X(t) < 0.5$.

at.% Nb	Normalizing $X(t_{end})$	n_1	$n_1 lnk_1$	r	g	k_1 10^{-3} s^{-1}
3	1	1.140(2)	−6.76(1)	0.9996	0.071	2.7
	< 1	1.082(3)	−6.61(2)	0.9990	0.052	2.2
5	1	1.007(4)	−6.243(2)	0.99998	0.029	2.0
	< 1	0.965(1)	−6.201(5)	0.9998	0.016	1.6

However, Eq. (10) cannot be directly applied to the data. Experimental data are noisy and Eq. (10) needs derivatives, which will even increase the noise. In order to handle smoother data, crystalline fraction (normalized to the saturation value at isothermal treatment) was fitted to Eq. (6) assuming $\alpha_{cr}/\alpha_{cr}^{sat} = X_\gamma$ and $X_{ext} = k(t - t_0)$ (i.e. $n = 1$ for simplification). On the other hand, the average crystallite volume was fitted to $\langle V_{cr} \rangle = at^b$, taken as the simplest curve resembling the evolution of this parameter. The data and the fitting curve are shown in Fig. 11. Fitting results of α_{cr} are $\alpha_{cr}^{sat} = 34(4)$ %, $k = 1.46(10)\cdot10^{-4}$ s^{-1}, $\gamma = 1.5(4)$ and $t_0 = 0.96(12)\cdot10^3$ s. It can be observed that γ is in agreement with the expected value (see Fig. 4). In the case of $\langle V_{cr} \rangle$, fitting parameters are $a = 73(8)$ nm^3s^{-b} and $b = 0.252(13)$.

Application of Eq. (10) (which is independent of the kinetic model) to these data is shown in Fig. 12. The nucleation rate ,$I(t)$, decreases as time increases during isothermal treatment, even after normalization of available space for nucleation using the saturation value of the crystalline fraction. This can be understood as the amorphous matrix becomes progressively enriched in elements non-soluble in the α-Fe(Si) phase (Nb and B) increasing the activation energy for nucleation and thus reducing $I(t)$ as the isothermal transformation progresses. In fact, once $I(t)$ is plotted vs. the transformed fraction (inset of Fig. 12) a linear decrease with α_{cr}=$\alpha_{cr}^{sat}X$ is found: $I(\alpha_{cr}) = 271(1) - 9.4(3)\alpha_{cr}$ $\mu m^{-3}s^{-3}$ (with α_{cr} in %) or $I(X) = 271(1)[1 - 1.2(4)X]$. In this second expression the close to 1 value of the prefactor of X points to a nucleation site exhaustion as a plausible mechanism for the stop of the nanocrystallization process. As described above, this decreasing behavior of $I(t)$ yields slight underestimations of n of about 5 %.

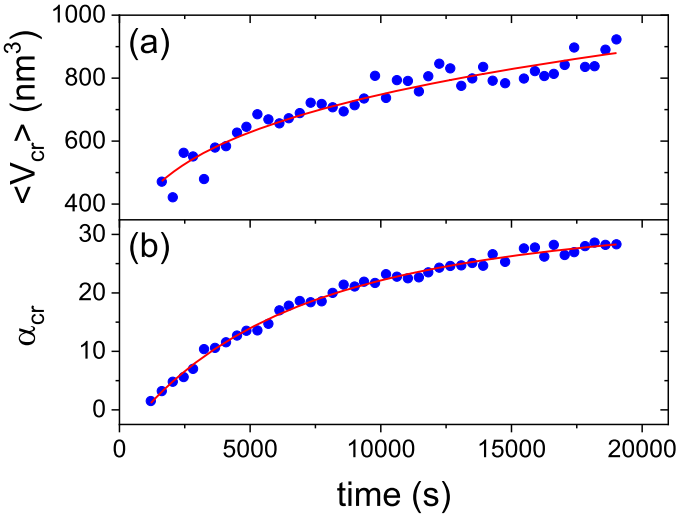

Fig. 11. Average size of nanocrystals, $\langle V_{cr} \rangle$, (a) and crystalline fraction, α_{cr}, (b) as a function of time during the isothermal treatment at 748 K. Symbols correspond to synchrotron X-ray diffraction [26]. Red lines correspond to fitting curves: $\langle V_{cr} \rangle = V_0 t^b$ and $\alpha_{cr} = \alpha_{cr}^{sat} X_\gamma$ (see Eq. 6).

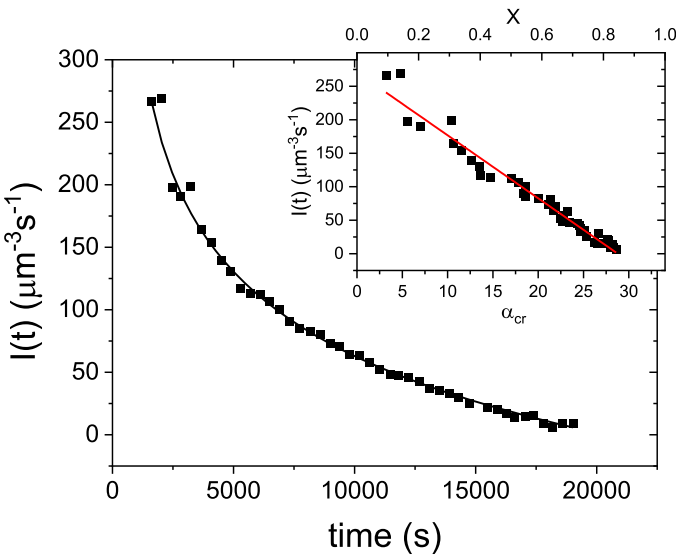

Fig. 12. Nucleation rate, $I(t)$, for the nanocrystallization of a FINEMET alloy from application of Eq. (10) to data shown in Fig. 11 (symbols) as a function of the isothermal time at 748 K (main panel) and as a function of the crystalline fraction (inset lower x-axis) and transformed fraction (inset upper x-axis). The black line in main panel corresponds to the smoothed curve obtained from the fit curves used in Fig. 11. The red line in inset corresponds to linear fitting of the data.

4. Conclusions

In the frame of nucleation and growth KJMA classical theory, decelerated growth processes cannot be correctly interpreted due to overgrowth problem. Theoretically, overgrowth occurs for any transformation with growth exponent $g < 1$. However, the simulations performed showed that overgrowth effects are almost negligible for diffusion controlled growth, for which the radius of a transformed region not submitted to impingement is expected to grow as the root square of time since its nucleation (growth exponent, $g = 1/2$). Smaller values of g yields deviations from KJMA theory only for very low values of g. Particularly, values close to $g = 0$ (instantaneous growth processes) yield artifacts such as double slope behavior of KJMA plot. Moreover, the non-constancy of the nucleation rate may introduce slight underestimation of the Avrami exponent.

From the analysis of the simulation results we have proposed simple procedures to acquire physically meaningful information from the application of KJMA plot. The correlation between the effective and the actual kinetic parameters is given and coherency is found with other kinetic models that assume a stronger impingement than the simple geometrical one considered in KJMA theory.

Application of the results derived from the simulations to the experimental data of nanocrystallization of FINEMET-type alloys allows us to estimate a growth exponent of ~ 0.06 that decreases to ~ 0.02 for alloys with a higher content of Nb. The nucleation rate was found to linearly decrease with the transformed fraction pointing to an exhaustion of nucleation at the end of the transformation. This can be related to the progressive enrichment in B and Nb of the amorphous matrix, which becomes stabilized, as the nanocrystallization progresses.

CRediT authorship contribution statement

J.S. Blázquez: Conceptualization; Data curation; Methodology; Simulations; Experiments; Writing-Original draft; Resources; Supervision. **R. Caballero-Flores:** Data curation; Methodology; Simulations; Writing-Original draft. **A.F. Manchón-Gordón:** Experiments; Writing-Reviewing and Editing. **J.M. Borrego:** Experiments; Writing-

Reviewing and Editing. **C.F. Conde:** Supervision; Writing- Reviewing and Editing; Resources.

Declaration of Competing Interest

The authors declare that they have no known competing financial interests or personal relationships that could have appeared to influence the work reported in this paper.

Data availability

Data will be made available on request.

Acknowledgements

This work was supported by the PAI of the Regional Government of Andalucía and the VI and VII PPI-US and by Junta de Andalucía-Consejería de Conocimiento, Investigación y Universidad (project ProyExcel_00360)

References

[1] A. N. Kolmogorov, Bull. Acad. Sci. USSR, Phys. Ser. 1937, 1, 355 [in Russian]. Selected Works of A. N. Kolmogorov, edited by A. N. Shiryayev, Vol.2 (Kluwer, Dordrecht, 1992), English translation, p. 188.
[2] W.A. Johnson, R.F. Mehl, Trans. Am. Inst. Mining Met. Engrs. 135 (1939) 416.
[3] M. Avrami, J. Chem. Phys. 9 (1941) 177.
[4] J.S. Blázquez, F.J. Romero, C.F. Conde, A. Conde, Phys. Stat. Sol. B 259 (2022), 2100524, https://doi.org/10.1002/pssb.202100524.
[5] A.A. Burbelko, E. Fras, W. Kapturkiewicz, Mater. Sci. Eng. A 413 (2005) 429–434, https://doi.org/10.1016/j.msea.2005.08.161.
[6] A.F. Manchón-Gordón, J.S. Blázquez, C.F. Conde, A. Conde, J. All. Compd. 675 (2016) 81–85, https://doi.org/10.1016/j.jallcom.2016.03.087.
[7] J.S. Blázquez, C.F. Conde, A. Conde, Int. J. Therm. Sci. 88 (2015) 1–6, https://doi.org/10.1016/j.ijthermalsci.2014.09.004.
[8] J.S. Blázquez, A.F. Manchón-Gordón, J.J. Ipus, C.F. Conde, A. Conde, Metals 8 (2018) 450, https://doi.org/10.3390/met8060450.
[9] A.F. Manchón-Gordón, R. López-Martín, J.J. Ipus, J.S. Blázquez, P. Svec, C. F. Conde, A. Conde, Metals 11 (849) (2021), https://doi.org/10.3390/met11060849.
[10] J. Christian, The Theory of Transformations in Metals and Alloys, Pergamon Elsevier Science, Oxford, 2002.
[11] M. Tomellini, M. Fanfoni, Phys. A-Stat. Mech. & Appl. 590 (2022), 126748, https://doi.org/10.1016/j.physa.2021.126748.
[12] M. Tomellini, M. Fanfoni, Eur. Phys. J. B 34 (2003) 331–341, https://doi.org/10.1140/epjb/e2003-00229-9.
[13] M. Tomellini, M. Fanfoni, Phys. A-Stat. Mech. & Appl. 333 (2004) 65–70, https://doi.org/10.1016/j.physa.2003.09.066.
[14] M. Tomellini, J. Mater. Sci. 48 (2013) 5653–5663, https://doi.org/10.1007/s10853-013-7361-2.
[15] G.A. Jones, P. Bonnett, S.F.H. Parker, J. Mag. Mag. Mat. 58 (1986) 216–226, https://doi.org/10.1016/0304-8853(86)90440-3.
[16] A.H. Taghvei, J. Eckert, J. All. Compd. 675 (2016) 223–230, https://doi.org/10.1016/j.jallcom.2016.03.053.
[17] J.S. Blázquez, C.F. Conde, A. Conde, Appl. Phys. A 76 (2003) 571–575, https://doi.org/10.1007/s00339-002-1664-5.
[18] M.J. Starink, J. Mater. Sci. 32 (1997) 4061–4070.
[19] J.B. Austin, R.L. Rickett, Trans. Am. Inst. Mining Met. Engrs. 135 (1939) 396.
[20] T. Tagami, S.I. Tanaka, J. Mater. Sci. 4 (355) (1999), https://doi.org/10.1023/A:1004474126385.
[21] A.F. Manchón-Gordón, J.S. Blázquez, C.F. Conde, A. Conde, J. Alloys Compd. 675 (2016) 81–85.
[22] V. M. Fokin, A. Cabral Jr., M. L. F. Nascimento, Ed. D. Zanotto, J. Sesták. On the Application of DTA/DSC Methods for the Study of Glass Crystallization Kinetics. In: Some Thermodynamic, Structural and Behavioral Aspects of Materiais Accentuating Non-crystalline States. J. Sesták M. Holocek, J. Málek, Eds. (2009) 286-306.
[23] J.M. Barandiarán, I. Tellería, J.S. Garitaonandía, H.A. Davies, J. Non-Cryst. Solids 329 (2003) 57–62, https://doi.org/10.1016/j.jnoncrysol.2003.08.013.
[24] A. Cerezo, M. Abraham, P. Clifton, H. Lane, D.J. Larson, A.K. Petford-Long, M. Thuvander, P.J. Warren, G.D.W. Smith, Micron 32 (2001) 731–739, https://doi.org/10.1016/S0968-4328(00)00080-9.
[25] K. Hono, D.H. Ping, Mater. Charact. 44 (2000) 203–217, https://doi.org/10.1016/S1044-5803(99)00047-9.
[26] J.M. Borrego, C.F. Conde, M. Millán, A. Conde, M.J. Capitán, J.L. Joulaud, Nanostruc. Mater. 10 (1998) 575–583.